Journal of Power Sources 248 (2014) 1156–1162

Contents lists available at ScienceDirect

Journal of Power Sources

journal homepage: www.elsevier.com/locate/jpowsour

Highly durable Pt/graphene oxide and Pt/C hybrid catalyst for polymer electrolyte membrane fuel cell

Ju Hae Jung, Hyang Jin Park, Junbom Kim, Seung Hyun Hur*

School of Chemical Engineering, University of Ulsan, Daehak-ro 93, Nam-gu, Ulsan 680-749, Republic of Korea

HIGHLIGHTS

- The durability of commercial catalyst is doubled by the addition of Pt/graphene oxide (GO).
- GO prevents the agglomeration of Pt in Pt/C catalyst by offering an anchoring site of eluted metal.
- The hybrid catalyst exhibits excellent durability especially in the high current region in the full cell test.

ARTICLE INFO

Article history:
Received 26 August 2013
Received in revised form
10 October 2013
Accepted 14 October 2013
Available online 21 October 2013

Keywords:
Polymer electrolyte membrane fuel cell
Graphene oxide
Accelerated durability test
Carbon corrosion

ABSTRACT

We report a highly durable hybrid catalyst composed of Pt/graphene oxide (GO) and Pt/C catalyst for polymer electrolyte membrane fuel cell (PEMFC). The accelerated durability tests in half-cell and full cell systems shows that the addition of small amount of Pt/GO catalyst significantly enhances the durability of commercial Pt/C catalyst without sacrificing initial electrochemical active surface area (ECSA). The XRD and TEM analysis reveal that the GO not only exhibits the high resistance to Pt agglomeration but also prevents the Pt agglomeration in Pt/C catalyst by providing the anchoring sites of eluted metal ions. We believe that this simple and effective approach can open a new way to fabricate highly durable electrocatalyst for the commercialization of fuel cell vehicles.

1. Introduction

Polymer electrolyte membrane fuel cell (PEMFC) has been widely studied due to its harmful greenhouse gases such as CO_2, NO_x, SO_x, etc., while it generates non-polluting things such as electricity, water, and heat using the chemical energy of fuel and oxidant. Today, it has been regarded as one of the most environmentally friendly power sources for many applications that need low working temperature, solid electrolyte, fast start-up and high efficiency. Despite its various merits, the commercial application of PEMFCs is impeded by its low durability, high cost and difficulty in the water management [1–4]. In order to reduce the cost and use it in various applications, long-term durability is regarded as the one of the most important problems to be solved [5–12].

Platinum (Pt) catalysts supported on the high surface area carbon (C) material such as carbon black (CB) have been widely used as an electrocatalyst for PEMFCs, but CB can be easily oxidized as the potential of oxygen reduction reaction is closer to that of carbon oxidation. The oxidation of CB can cause the agglomeration and loss of Pt nanoparticles, resulting in a decrease of the electrochemical surface area and activity of the electrocatalysts [13–16]. So far, many attempts have been made to solve the durability problem by introducing robust materials as a catalyst support such as graphene and carbon nanotube (CNT) which exhibit highly ordered graphitic structure [17–19].

Graphene, which is a 2-D honeycomb lattice of single layer of carbon atom with a thickness of 0.34 nm, has been extensively investigated due to its outstanding properties such as excellent thermal and electrical conductivities, high electron transfer rate, and superior chemical resistance. Graphene can be fabricated by chemical or mechanical exfoliation of natural graphite, chemical vapor deposition (CVD), and epitaxial growth. [20–29]. Among them, the chemical exfoliation of graphite into graphene oxide (GO) is considered as the one of the most appropriate method to fabricate electrocatalysts for PEMFC due to its versatility of functional groups (epoxy, carboxylic and hydroxyl groups which can act as nucleation and anchoring sites of metal nanoparticles), low

* Corresponding author.
E-mail address: shhur@ulsan.ac.kr (S.H. Hur).

0378-7753/$ – see front matter © 2013 Elsevier B.V. All rights reserved.
http://dx.doi.org/10.1016/j.jpowsour.2013.10.055

material cost, and suitability for large-scale up [30–32]. Previous studies have shown that using GO as a supporting material for electrocatalyst can improve the oxygen reduction reaction (ORR) of the Pt, Pt–Metal alloy and non Pt catalyst, however using only 2D GO as a catalyst support can cause severe mass transfer problems in the membrane electrode assembly (MEA) of the full cell system [18,19,33–37].

Here, we report a highly durable hybrid catalyst composed of Pt/GO and commercial Pt/C catalysts. The hybrid catalyst exhibited improved durability without sacrificing electrochemical active surface area (ECSA) due to both the highly durable Pt/GO itself and suppressed Pt agglomeration in commercial Pt/C by the synergetic effects of Pt/GO. Atomic Force microscope (AFM), X-ray photoelectron spectroscopy (XPS), Raman spectra measurement (Raman), Thermogravimetric analysis (TGA), X-ray diffraction (XRD), Transmission electron microscope (TEM), and cyclic voltammetry (CV) analysis were conducted to investigate the properties of fabricated catalysts.

2. Experimental

2.1. Preparation of Pt/GO catalyst

Hummers method using $NaNO_3$, H_2SO_4, $KMnO_4$, and H_2O_2 was used to prepare the GO from expandable graphite (Grade 1721-Asbury Carbon) [27]. Firstly, the pre-calculated amount of metal precursor, $H_2PtCl_6{\cdot}xH_2O$ (Sigma–Aldrich Corporation, St. Louis, MO, USA) and 50 mg GO were dispersed in 200 mL ethyl glycol (EG, Daejung Chemicals, Republic of Korea), then the suspension was heated and stirred at 110 °C for 90 min to convert Pt precursor to Pt nanoparticles. The final product was collected by filtration followed by washing with ethanol and drying. To prepare catalyst ink, the fabricated catalysts were physically mixed with proper amount of nafion ionomer in isopropanol (IPA, Daejung Chemicals, Republic of Korea) solvent. The loading amount of Pt in Pt/GO catalyst was kept to 40 wt% for all experiments.

2.2. Preparation of the MEAs

MEAs were fabricated to evaluate the catalytic performances in the full cell system. The commercial 40.0 wt% Pt/C (HiSPEC™ 4000, Johnson Matthey) catalyst was used as the anode catalyst and the hybrid catalyst composed of commercial Pt/C and Pt/GO fabricated in this study was used as the cathode catalysts to prepare MEAs. The catalysts were mixed with a 5 wt% Nafion ionomer (Sigma–Aldrich, Inc.) and isopropanol (IPA) solution in order to make a slurry, which was then coated by decal process onto the polymer electrolyte membrane (Nafion-212 membrane) [30]. Catalyst was coated using the same procedure except with the 25 wt% Nafion ionomer. The Nafion ionomer content in the electrode was calculated using the following equation.

$$\text{Nafion content(wt\%)} = \frac{\text{Nafion weight}}{\text{Nafion weight} + \text{catalyst weight}} \times 100$$

The areas of both the anodes and cathodes were 25 cm^2 and 0.4 mg Pt cm^{-2} was loaded on each electrode.

2.3. Instrumental analysis

Atomic Force microscope (AFM, Veeco Dimension 3100) was used to measure the thickness of GO in tapping mode. AFM sample was prepared by drop-casting of low concentration of GO suspension on silicon wafer followed by drying in air at room temperature. X-ray photoelectron spectroscopy (XPS, Thermo Fisher K-alpha) was conducted to investigate the functional groups and chemical compositions of GO. Thermogravimetric analysis (TGA, TA Instruments TGA Q50) was used to determine the loading amount of Pt on the supporting materials by heating the catalysts to 900 °C with 10 °C min^{-1}. X-ray diffraction (XRD, Rigaku RAD-3C) was performed to investigate crystal structure and calculate the particle size of the Pt. XRD data were collected from 10 to 100° range with Cu Kα radiation (λ = 1.541 Å). Transmission electron microscope (TEM, JEOL JEM-2010) images were also collected to see the size and distribution of Pt nanoparticles on GO and CB.

2.4. Electrochemical analysis

The cyclic voltammetry (CV, BioLogic, SP-50) analysis was conducted to evaluate the electrocatalytic activity of Pt/C, Pt/GO, and Pt/GO-Pt/C hybrid catalysts with three-electrode half-cell system using Ag/AgCl reference electrode and Pt counter electrode in 0.5 M H_2SO_4 (aq.) as the electrolyte at 25 °C. The working electrode was prepared by casting 3 μl of catalyst ink onto a pre-polished glassy carbon disk (GC, 3 mm in diameter). The catalysts were mixed with a 5 wt% Nafion ionomer and IPA solution in order to make slurry, which was then casted on GC electrode. Nafion ionomer was used to protect detachment of the catalyst layer. The counter electrode was a GC plate, and an Ag/AgCl electrode was used as the reference electrode. The scan rate and scan range for general tests were 50 mV s^{-1} and −0.2 to 1.0 V, respectively. Durability of catalysts was compared after 60 min scan between 0.4 and 1.2 V with 50 mV s^{-1} scan rate to expose them to accelerated condition as the carbon corrosion occurs more quickly at higher potential.

Full-cell test was carried out in the following ways. Firstly, the MEA prepared in this study was assembled to cell fixture (Fuel Cell Technologies Co.) with gas diffusion layers (GDL) (JNTG, JEN-40-A2). Then, cell performance was evaluated under the hydrogen and air feeding in stoichiometric ratios of 1.5 and 2.0, respectively while the temperature was maintained at 343 K with 100% relative humidity at ambient pressure. CV measurements were carried out to evaluate the electrochemical active surface (ECSA) area at a scan rate of 50 mV s^{-1} supplying hydrogen and nitrogen to the anode and cathode, respectively. Durability of catalysts was compared after 3 h constant high voltage operation (1.4 V). ECSA of Pt nanoparticles was determined by calculating the hydrogen desorption area. The charge for monolayer desorption of hydrogen on Pt was assumed to be 210 μC cm^{-2}. All potentials, however, are referenced with respect to the reversible hydrogen electrode (RHE).

3. Results and discussion

3.1. Chemical and physical structures of carbon supports

AFM and XRD were used to confirm the exfoliation of graphite. As shown in Fig. 1(a), GO fabricated in this study shows well-exfoliated 1 nm thick single layer. The increased thickness of GO than that of graphene fabricated by CVD (~0.34 nm) can be attributed to functional groups and the defect of sp^3-hybridized carbon bonding generated during the oxidation of graphite [19,35,36]. As shown in Fig. 1(b), XRD patterns of natural graphite and GO exhibit peaks at around $2\theta = 26°$ and $2\theta = 11°$ corresponding to the (002) plane with d-spacing of 0.34 nm and 0.78 nm, respectively [18,38]. The increased interlayer spacing of GO than that of natural graphite is due to the intercalation of water molecules and generated oxygenated functional groups, such as epoxy and hydroxyl, between the intergalleries of the graphite sheets during severe oxidation. The loading amount of Pt on the carbon support was measured by TGA. It can be clearly seen that Pt/C and Pt/GO catalyst used in this experiments have similar amount of the Pt loading with 40.03 and 40.84 wt %, respectively [39].

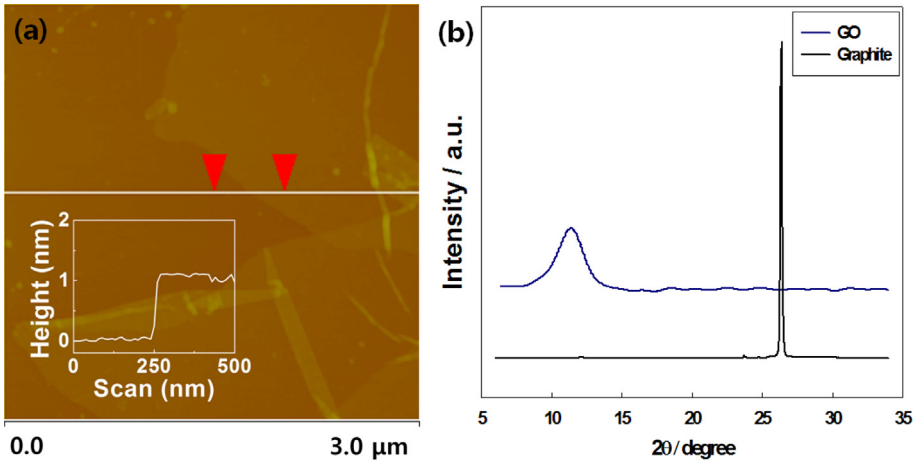

Fig. 1. (a) AFM image of GO and (b) XRD pattern of graphite and GO.

XPS was used to investigate the chemical structure of carbon in graphite, Pt/C, and Pt/GO. As shown in Fig. 2(a), the C1s XPS peak of GO can be de-convoluted into four types of peaks such as C–C, C–N, C–O, C=O, and O–C=O corresponding to the binding energy of 284.5, 285.6, 286.5, 287.5, and 288.6 eV, respectively, which indicates that high amount of oxidized functional groups including hydroxyl, epoxy, ketone, aldehyde, and carboxylic acids are present in GO [14,15]. Instead, C1s peak of Pt/GO shows the similar components but highly reduced functional groups than that of original GO, which indicates that Pt precursor reacted with the functional groups of GO during the deposition of Pt on the GO support [29]. Relatively low amount of functional groups are observed in commercial catalyst. Raman spectra of GO and Pt/GO are shown Fig. 2(g) to compare the chemical structure between them. Both samples exhibit the D and G band at same position around 1328 and 1595 cm^{-1}, respectively. The G band is the first order scattering of E_{2g} phonons of sp^2-hybridized carbon atoms and D peak is a breathing mode of j-point photons of A_1g symmetry of sp^3-hybridized carbon atoms of disordered graphene [40–42]. The I_D/I_G values of Pt/GO are increased to 1.23 from 0.95 for GO, which indicates the restoration of C=C bonds and the creation of numerous small sp^2 domains by the reduction of oxygen functional groups during the Pt loading step [40].

3.2. Electrochemical properties

The change of ECSA for various catalysts after 30, 60 min repeated CV scan in the half-cell system is shown in Fig. 3. The

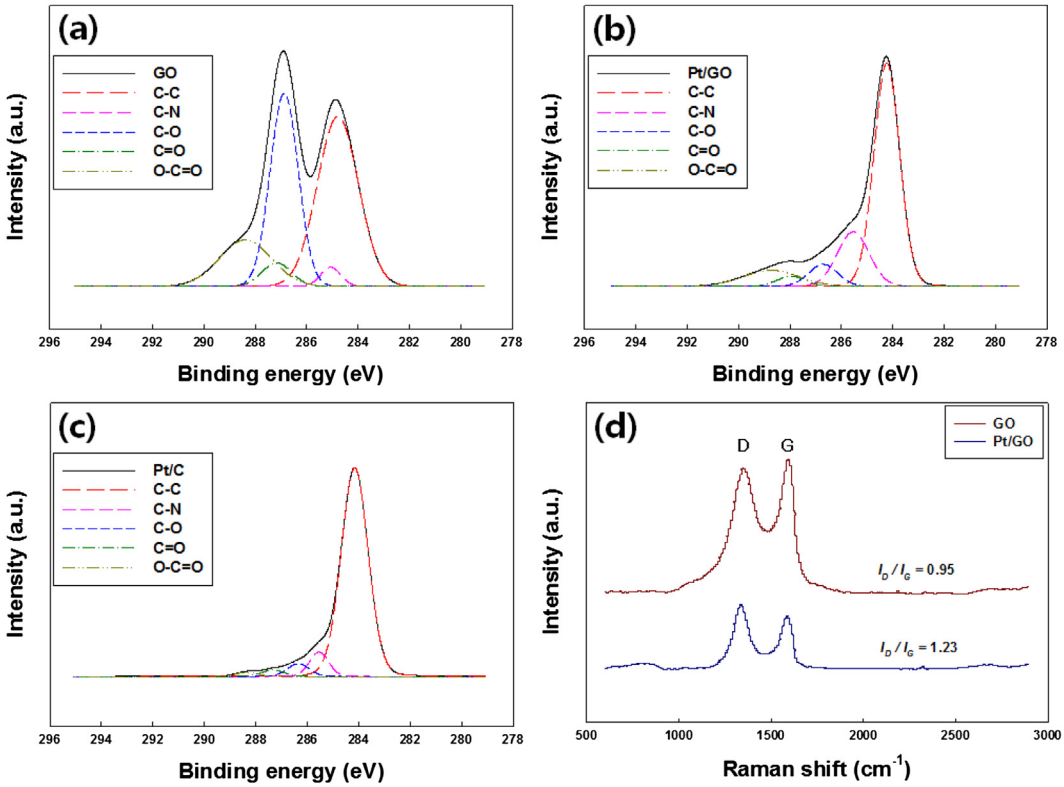

Fig. 2. XPS spectra of (a) GO, (b) Pt/GO, and (c) Pt/C. (d) Raman spectra of GO and Pt/GO.

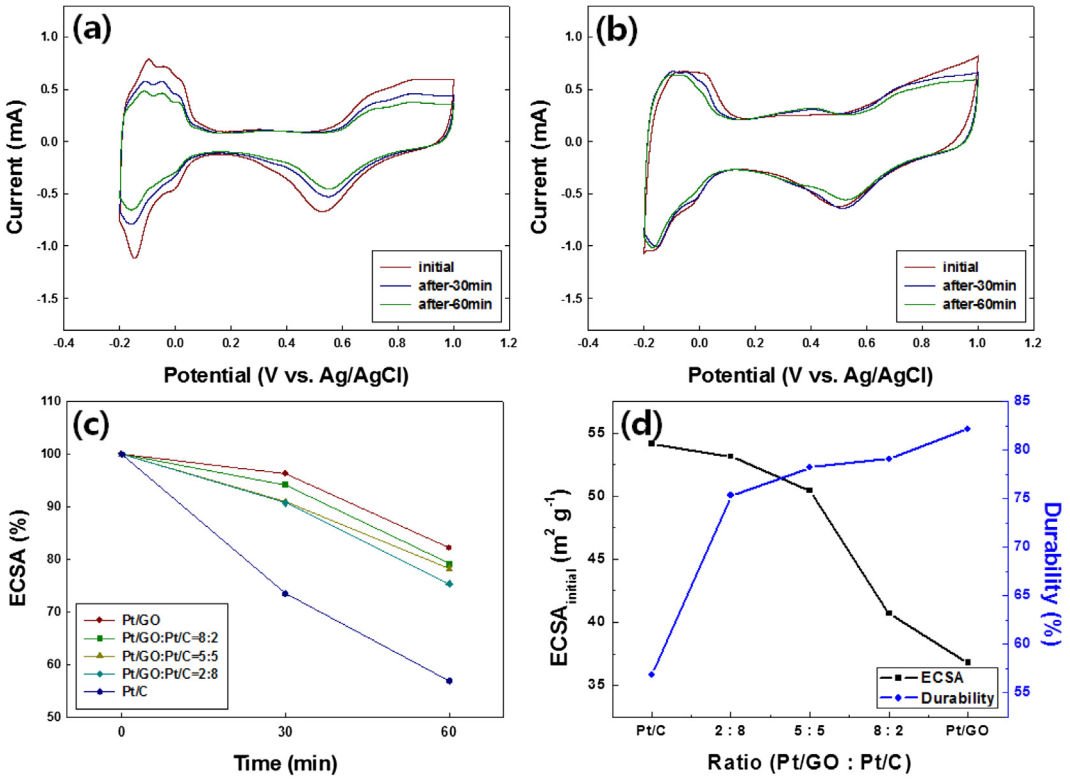

Fig. 3. Cyclic voltammograms (CVs) of (a) Pt/C and (b) Pt/GO. (c) Electrochemical active surface area (ECSA) change of various catalysts after 60 min high voltage CV cycles. (d) Initial ESCA and durability of various catalysts.

Table 1
Active surface area of each catalyst before and after acceleration test in half cell system.

Pt/GO:PtC	Active surface area (m^2 g^{-1})		
	Initial	After	
		30 min	60 min
Pt/C	54.21	39.83	30.82
Deactivation		−26.52%	−43.15%
2:8	53.16	48.23	40.04
Deactivation		−9.28%	−24.69 %
5:5	50.43	45.87	39.45
Deactivation		−9.04%	−21.78%
8:2	40.68	38.31	32.18
Deactivation		−5.83%	−20.89%
Pt/GO	36.79	35.39	30.24
Deactivation		−3.81%	−17.81%

commercial Pt/C catalyst exhibits the largest initial ECSA but the lowest durability among all catalysts tested. As summarized in Table 1, the ECSA of Pt/C was 54.21 m^2 g^{-1} initially but it rapidly dropped to 30.82 m^2 g^{-1} (−43.15%), instead, that of Pt/GO was 36.79 m^2 g^{-1} but it dropped only −17.81% (30.24 m^2 g^{-1}) after 60 min accelerated CV cycles. As the GO content increased in hybrid catalysts the initial ESCA decreased but the durability was significantly improved as shown in Fig. 3(d), which implies that there are synergetic effects between Pt/C and Pt/GO catalysts. It should be noted that the addition of relatively small amount of Pt/GO (20%) almost doubled the durability of commercial Pt/C catalyst without sacrificing the initial ECSA. Based on the degree of activity loss according to the Pt/GO content, we can deduce that GO not only shows the improved durability itself but also prevents the

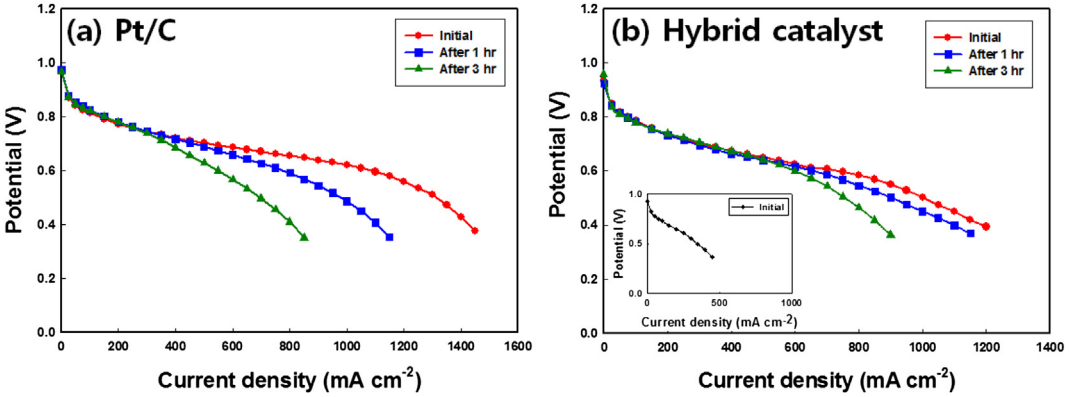

Fig. 4. Polarization curves of fabricated MEAs before and after accelerated durability test (ADT) for (a) Pt/C and (b) hybrid catalyst operated in full cell system. The inset shows polarization curves of fabricated MEAs for only Pt/GO catalyst.

Table 2
Current densities and ECSAs of the MEAs before and after accelerated durability test (ADT).

Sample	Current density (mA cm^{-2} @0.6 V)			ECSA (m^2 g^{-1})		
	Initial	After		Initial	After	
		1 h	3 h		1 h	3 h
Pt/C	1003.35	776.60	547.97	36.90	25.55	17.32
Deactivation		−22.6%	−45.4%		−30.8%	−53.1%
Hybrid cat.	727.23	652.53	598.04	26.91	21.67	19.80
Deactivation		−10.3%	−17.7%		−19.5%	−26.4%

Table 3
Mean particle size and agglomeration ratio of catalysts after ADT measured by XRD and TEM.

Sample	XRD			TEM		
	Pt particles size (nm)		Agglomeration ratio	Pt particles size (nm)		Agglomeration ratio
	Initial	After 3 h		Initial	After 3 h	
Pt/C	3.0	8.0	+167%	3.2	8.6	+169%
Hybrid catalyst	2.8	5.3	+89%	2.9	4.9	+69%

agglomeration and the loss of Pt nanoparticles in Pt/C catalyst [14,18].

At elaborated temperature, due to the high water uptake, high oxygen content, low pH, and high potential, there is activity loss due to the oxidation of carbon support. The carbon corrosion leads to weakening of boding strength of Pt particles to carbon support due to the structural collapse of carbon materials [43]. Recently, it has been reported that the graphitic carbon material such as carbon nanotubes (CNTs), graphene nanoplatelets and GOs exhibit highly improved corrosion resistance due to their excellent electrical conductivity, high chemical stability, and mechanical strength [44,45]. The high carbon crystallinity of Pt/GO used in this study is believed to improve the electrochemical stability in the hybrid catalyst.

To investigate the synergetic effects further, accelerated deactivation test (ADT) was also carried out in full cell system by applying high voltage (1.4 V) for 3 h. As shown in Fig. 4, MEA fabricated with commercial Pt/C shows higher initial electrochemical current (1003.35 mA cm^{-2} at 0.6 V) than that with hybrid catalysts (Pt/C:Pt/GO = 8:2, 727.23 mA cm^{-2} at 0.6 V). However, it exhibited inferior durability (45.4% activity loss) to hybrid catalyst (17.7% activity loss) as summarized in Table 2 after 3 h ADT. It is well known that the activity loss at low current region (ohmic region) is due to the increase of i) ion flow resistance in the electrolyte and ii) electron transfer resistance through the electrically conductive fuel cell components [32], and that at high current region (mass transfer limit region) is due to the agglomeration or loss of Pt nanoparticles induced by the carbon corrosion [13]. As it can be clearly seen from Fig. 4 that main activity loss occurs in high current region,

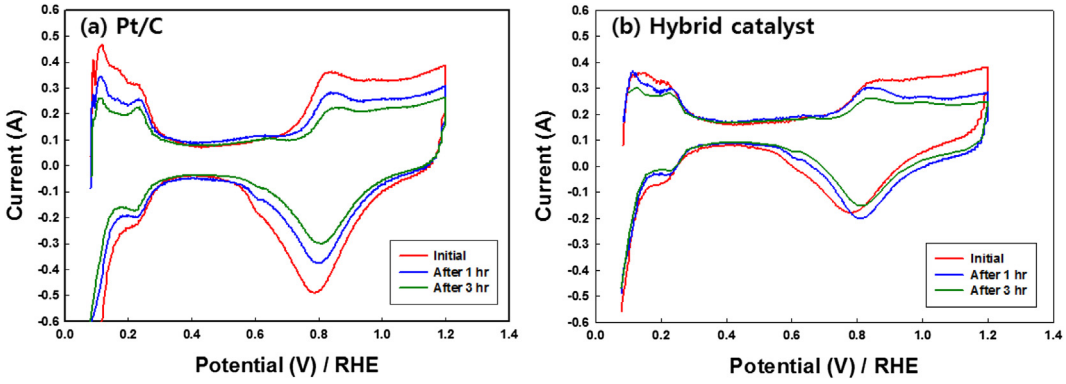

Fig. 5. Cyclic voltammograms of fabricated MEAs before and after accelerated durability test (ADT) for (a) Pt/C and (b) hybrid catalyst operated in full cell system.

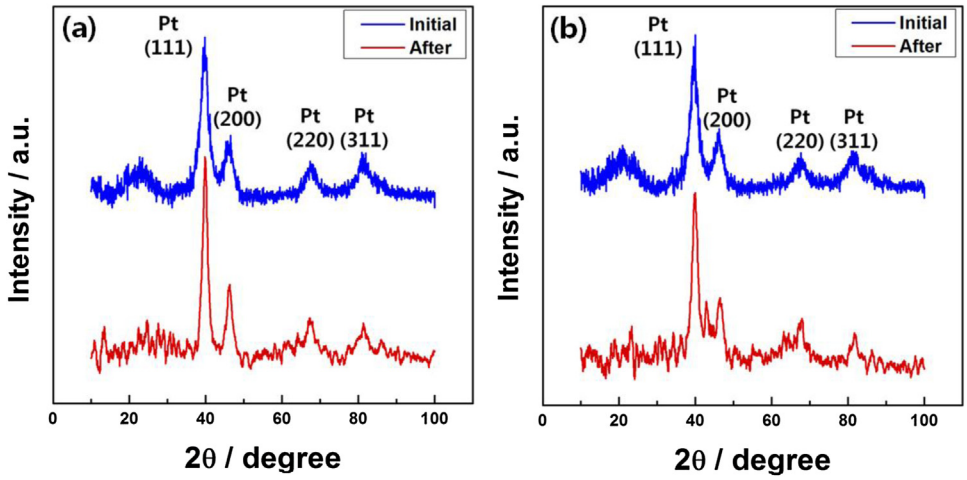

Fig. 6. XRD patterns of catalyst before and after accelerated durability test (ADT) for (a) Pt/C and (b) hybrid catalyst.

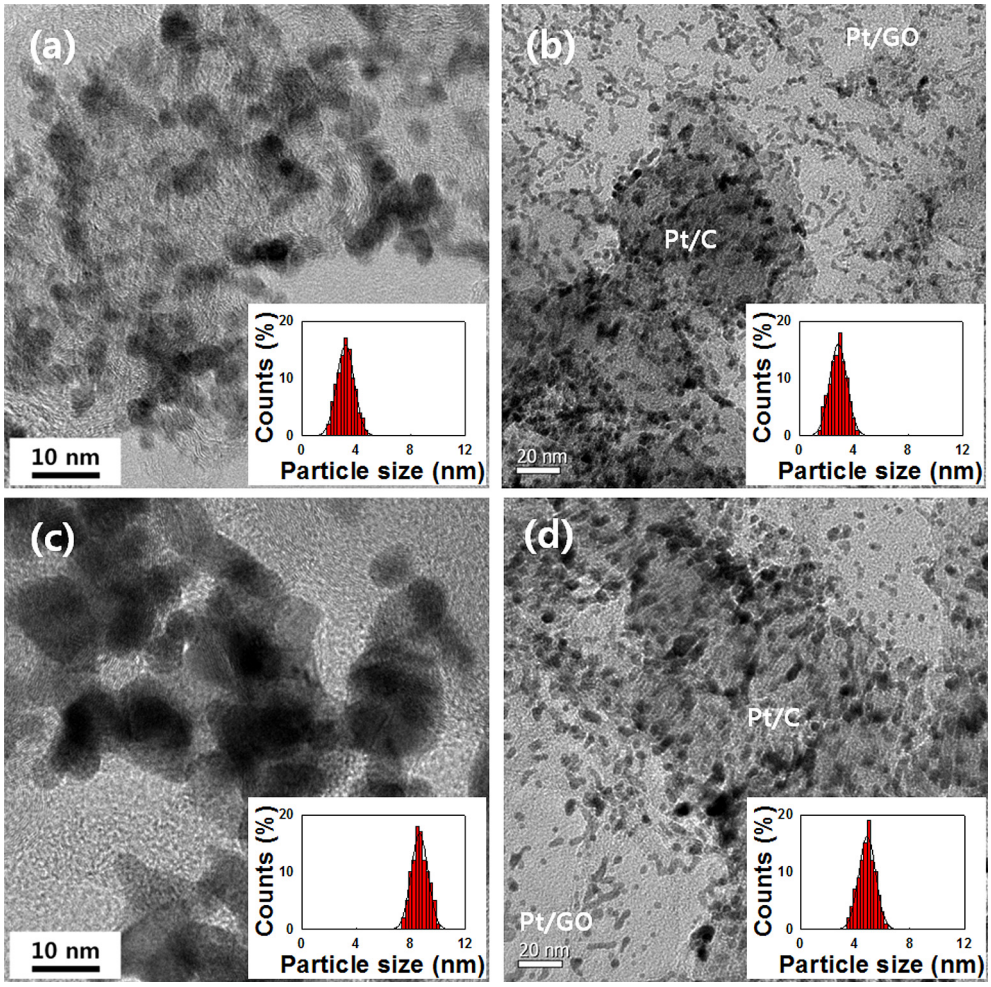

Fig. 7. TEM images and their corresponding particle size histograms of initial (a) Pt/C and (b) hybrid catalyst. TEM images final (c) Pt/C and (d) hybrid catalyst after accelerated durability test.

which indicates that GO impeded the agglomeration and loss of Pt nanoparticles in case of hybrid catalyst.

CV results for the cathode side in full cell system are shown in Fig. 5 before and after ADT. Similar as half-cell results, Pt/C showed larger initial ECSA and electric double layer thickness than those of hybrid catalyst, which is well correlated with the higher initial activity of Pt/C catalyst over hybrid catalyst. However, as summarized in Table 2, ECSA of the Pt/C was decreased 53.1% from 36.90 to 17.32 $m^2\ g^{-1}$ while that of hybrid catalyst decreased only 26.4% from 26.91 to 19.80 $m^2\ g^{-1}$ after 3 h ADT, which also means that addition of Pt/GO prevented the agglomeration of Pt nanoparticles and thus retained ECSA better.

To calculate the Pt particle precisely by Scherrer's equation [15], XRD was taken and shown in Fig. 6. The sharp diffraction peaks of Pt crystalline structure that can be correlated to (111), (200), (220) and (311) planes are shown and broad peak at around 25° that is related to carbon supports is also observed. As summarized in Table 3, the average Pt size of Pt/C catalyst increased 167% from 3.0 to 8.0 nm, instead, that of hybrid catalyst increased 89% from 2.8 to 5.3 nm, which is well correlated with ESCA comparison both in half-cell and full cell test after 3 h ADT. Agglomeration ratio is a ratio describing how many percentages of Pt nanoparticles agglomerate after 3hr ADT.

To see the effect Pt growth in hybrid catalyst in detail during ADT, TEM images were collected for each catalyst. As shown in Fig. 7(a) and (b), Pt nanoparticles are well dispersed on CB and GO surface with 2–4 nm size initially. After ADT, high degree of agglomeration was observed in Pt/C catalyst (Fig. 7(c)), instead, only small amount of agglomeration was observed both GO and CB support in the hybrid catalyst, which indicates that GO prevent the Pt growth not only in itself but also in CB.

In general, the Pt particle grows through Ostwald ripening process in commercial Pt/C catalyst. Pt particles are dissolved during the cell operation by the carbon corrosion and then they are re-loaded or re-impregnated again on the remaining Pt particles, which results in agglomeration and large Pt particles [46,47]. The GO present in the hybrid catalyst has many kinks, defects, and functional groups which can offer the active site for nucleation or collects of Pt eluted from Pt/C, which can be resulted in the less agglomeration of Pt even in the CB support [48]. The GO produced by the functionalization process inherits a lot of defect sites, and we believe that the defect sites strongly anchor the Pt nanoparticles and prevent them from aggregating or dissolving into the electrolyte during sulfuric acid electro-oxidation.

4. Conclusions

The durability of commercial Pt/C catalyst was improved by the addition of Pt/GO catalyst without sacrificing initial electrochemical activity. The high voltage CV cycle test in half-cell system

revealed that as the Pt/GO content increased, the initial ECSA decreased but durability was highly improved. When 20% Pt/GO was mixed with commercial Pt/C catalyst, the durability doubled while only 2% initial ECSA dropped. The hybrid catalyst also showed about 3 fold higher durability than that of commercial Pt/C catalyst in full cell accelerated durability test especially at high current region. XRD and TEM analysis revealed that GO prevented the agglomeration of Pt in Pt/C catalyst by offering anchoring site of eluted metal, which resulted in the more enhancement in durability than that based on its content.

Acknowledgments

This research was supported by the Basic Science Research Program through the National Research Foundation of Korea (NRF) funded by the Ministry of Education, Science and Technology (2013R1A1A2A10004468).

References

[1] A. Ohma, S. Yamamoto, K. Shinihara, J. Power Sources 182 (2008) 39–47.
[2] M.A. Rubio, A. Urquia, S. Dormido, Int. J. Hydrogen Energy 35 (2010) 2586–2590.
[3] J.H. Jung, B.I. Park, J.B. Kim, Nanoscale Res. Lett. 7 (2012) 34–41.
[4] S. Sun, G. Zhang, D. Geng, Y. Chen, R. Li, M. Cai, X. Sun, Angew. Chem. Int. Ed. 123 (2011) 442–446.
[5] Y. Shoa, G. Yin, Y. Gao, J. Power Sources 171 (2007) 558–566.
[6] S. Sharma, B.G. Pollet, J. Power Sources 208 (2012) 96–119.
[7] Y. Zhang, R. Pitchumani, Int. J. Heat Mass Transfer 50 (2007) 4698–4712.
[8] S. Zhang, X. Yuan, H. Wang, W. Mérida, H. Zhu, J. Shen, S. Wu, J. Zhang, Int. J. Hydrogen Energy 34 (2009) 388–404.
[9] C.W.B. Bezerra, L. Zhang, H. Liu, K. Lee, A.L.B. Marques, E.P. Marques, H. Wang, J. Zhang, J. Power Sources 173 (2007) 891–908.
[10] N. Yousfi-Steiner, P. Moctéguy, D. Candusso, D. Hissel, J. Power Sources 194 (2009) 130–145.
[11] S. Giddey, F.T. Ciacchi, S.P.S. Badwal, V. Zelizko, J.H. Edwards, G.J. Duffy, Solid State Ionics 152–153 (2002) 363–371.
[12] R.I. Jafri, T. Arockiados, N. Rajalakshmi, S. Ramaprabhua, J. Electrochem. Soc. 157 (2010) B874–B879.
[13] J.H. Jung, M.S. Cha, J.B. Kim, J. Nanosci. Nanotechnol. 12 (2012) 5412–5417.
[14] S.H. Kim, T.K. Lee, J.H. Jung, J.N. Park, J.B. Kim, S.H. Hur, Mater. Res. Bull. 47 (2012) 2760–2767.
[15] T.K. Lee, J.H. Jung, J.B. Kim, S.H. Hur, Int. J. Hydrogen Energy 37 (2012) 17992–18000.
[16] J.G. Oh, W.H. Lee, H.S. Kim, Int. J. Hydrogen Energy 37 (2012) 2455–2461.
[17] F. Maillard, A. Bonnefont, F. Micoud, Electrochem. Commun. 13 (2011) 1109–1111.
[18] C.V. Rao, A.L.M. Reddy, Y. Ishikawa, P.M. Ajayan, Carbon 49 (2011) 931–936.
[19] R. Kou, Y. Shao, D. Wang, M.H. Engelhard, J.H. Kwak, J. Wang, V.V. Viswanathan, C. Wang, Y. Lin, Y. Wang, I.A. Aksay, J. Liu, Electrochem. Commun. 11 (2009) 954–957.
[20] A.K. Geim, K.S. Novoselov, Nat. Mater. 6 (2007) 183–191.
[21] E. Antolini, Appl. Catal. B Environ. 123–124 (2012) 52–68.
[22] H. Oh, J. Lee, H. Kim, Int. J. Hydrogen Energy 37 (2012) 10844–10849.
[23] Y. Xin, J. Liu, X. Jie, W. Liu, F. Liu, Y. Yin, J. Gu, Z. Zou, Electrochim. Acta 60 (2012) 354–358.
[24] Y. Xin, J. Liu, Y. Zhou, W. Liu, J. Gao, Y. Xie, Y. Yin, Z. Zou, J. Power Sources 196 (2011) 1012–1018.
[25] E. Yoo, T. Okata, T. Akita, M. Kohyama, J. Nakamura, I. Honma, Nano Lett. 9 (2009) 2255–2259.
[26] B. Seger, P.V. Kamat, J. Phys. Chem. C 113 (2009) 7990–7995.
[27] W.S. Hummers, R.E. Offeman, J. Am. Chem. Soc. 80 (1958) 1339.
[28] F. Ali, N. Agarwal, P.K. Nayak, R. Das, N. Periasamy, Curr. Sci. 97 (2009) 683–685.
[29] T.K. Lee, H.J. Park, M.K. Kwon, J.H. Jung, J.B. Kim, S.H. Hur, J. Nanomater. 2012 (2012) 1–6.
[30] A. Lerf, H. He, M. Forster, J. Klinowski, J. Phys. Chem. B 102 (1998) 4477–4482.
[31] C.Y. Ahn, J.Y. Cheon, S.H. Joo, J.B. Kim, J. Power Sources 222 (2013) 477–482.
[32] R. O'Hayre, S.W. Cha, W. Colella, F.B. Prinz, Fuel Cell Fundamentals, John Wiley & Sons, Hoboken, 2006.
[33] J. Maruyama, I. Abe, J. Power Sources 178 (2005) 1–8.
[34] K.O. Maeda, Y. Morikawa, S. Tanaka, M. Kohyama, Surf. Sci. 604 (2010) 144–154.
[35] Y. Okamoto, Chem. Phys. Lett. 420 (2006) 382–386.
[36] Y. Okamoto, Chem. Phys. Lett. 407 (2005) 354–357.
[37] C. Aribizzani, S. Righi, F. Soavi, M. Mastragostino, Int. J. Hydrogen Energy 36 (2011) 5038–5046.
[38] M.J. McAllister, J.L. Li, D.H. Adamson, H.C. Schniepp, A.A. Abdala, J. Liu, H.A. Margarita, D.L. Milius, R. Car, R.K. Prud'homme, I.A. Aksay, Chem. Mater. 19 (2007) 4396–4404.
[39] S. Stankovich, D.A. Dikin, R.D. Piner, K.A. Kohlhaas, A. Kleinhammes, Y. Jia, Y. Wu, S.T. Nguyen, R.S. Ruoff, Carbon 45 (2007) 1558–1565.
[40] B. Saner, F. Okyay, Y. Yurum, Fuel 89 (2010) 1903–1910.
[41] J.M. Englert, J. Rohrl, C.D. Schmidt, R. Graupner, M. Hundhausen, F. Hauke, A. Hirsch, Adv. Mater. 21 (2009) 4265–4269.
[42] S. Amini, H. Kalaantari, J. Garay, A.A. Balandin, R. Abbaschian, J. Mater. Sci. 46 (2011) 6255–6263.
[43] S. Zhang, X. Yuan, J. Cheng Hin, H. Wang, K.A. Friedrich, M. Schulze, J. Power Sources 194 (2009) 588–600.
[44] N. Liu, F. Luo, H. Wu, Y. Liu, C. Zhang, J. Chen, Adv. Funct. Mater. 18 (2008) 1518–1525.
[45] Y. Shao, S. Zhang, C. Wang, Z. Nie, J. Liu, Y. Wang, Y. Lin, J. Power Sources 195 (2010) 4600–4605.
[46] C.G. Chung, L. Kim, Y.W. Sung, J.W. Lee, J.S. Chung, Int. J. Hydrogen Energy 34 (2009) 8974–8981.
[47] Z. Xu, H. Zhang, H. Zhong, Q. Lu, Y. Wang, D. Su, Appl. Catal. B Environ. 111 (2012) 264–270.
[48] Y. Li, Y. Li, E. Zhu, T. Mclouth, C.Y. Chiu, X. Huang, Y. Huang, J. Am. Chem. Soc. 134 (2012) 12326–12329.